Feasibility of *in vivo* intravascular photoacoustic imaging using integrated ultrasound and photoacoustic imaging catheter

Andrei B. Karpiouk
Bo Wang
James Amirian
Richard W. Smalling
Stanislav Y. Emelianov

Feasibility of *in vivo* intravascular photoacoustic imaging using integrated ultrasound and photoacoustic imaging catheter

Andrei B. Karpiouk,[a] Bo Wang,[a] James Amirian,[b] Richard W. Smalling,[b] and Stanislav Y. Emelianov[a]
[a]University of Texas at Austin, Department of Biomedical Engineering, Austin, Texas 78712
[b]University of Texas Health Science Center, Division of Cardiology, Houston, Texas 77030

Abstract. Pilot studies of *in vivo* combined intravascular ultrasound (IVUS) and intravascular photoacoustic (IVPA) imaging are reported. A recently introduced prototype of an integrated IVUS/IVPA imaging catheter consisting of a single-element ultrasound transducer and a light delivery system based on a single optical fiber was adapted and used for *in vivo* imaging of a coronary stent deployed in a rabbit's thoracic aorta in the presence of luminal blood. The results suggest that *in vivo* IVUS/IVPA imaging is feasible using the integrated IVUS/IVPA imaging catheter. The challenges of *in vivo* combined IVUS/IVPA imaging are discussed, and further improvements on the design of the catheter and the clinical imaging system are proposed. © *2012 Society of Photo-Optical Instrumentation Engineers (SPIE).* [DOI: 10.1117/1.JBO.17.9.096008]

1 Introduction

Intravascular ultrasound (IVUS) imaging is a clinically approved catheter-based minimally invasive imaging tool used in the visualization, characterization and treatment guidance of atherosclerotic arteries. IVUS is a real-time imaging modality allowing for the imaging of the arterial wall with a resolution of under 150 μm.[1] While the morphology of the arterial tissues can be visualized, IVUS by itself cannot reliably characterize tissue composition due to insufficient acoustic contrast among various types of tissues. To overcome this limitation, a photoacoustic characterization of arterial tissues has been investigated.[2–5] In photoacoustic imaging, which is being explored for a wide range of biomedical applications,[6] the contrast is based on differences of light absorption of various tissues. Short laser pulses are absorbed by tissues and converted into heat due to fast nonradiative relaxation.[7,8] The thermal expansion of heated tissues generates photoacoustic transients that can be detected by the same ultrasound transducer used for ultrasound imaging. Given the synergy of ultrasound and photoacoustic imaging, ultrasound-guided intravascular photoacoustic (IVPA) imaging[9,10] capable of identifying tissue composition based on tissue's optical properties has been demonstrated.[11–13] Furthermore, imaging contrast agents were explored to identify molecular and cellular signatures associated with atherosclerosis.[14–18] Compared to IVUS imaging, IVPA has a similar imaging depth of several millimeters and imaging resolution within one hundred micrometers.[10] IVPA imaging was combined with IVUS imaging thus visualizing both morphology and composition of soft tissues. Recently, combined IVUS/IVPA imaging was used *ex vivo* to characterize plaque composition including lipid and macrophages.[11,12,15–19]

In vivo IVUS/IVPA imaging can be performed using an integrated IVUS/IVPA imaging catheter capable of both delivering pulsed laser irradiation into an arterial lumen with consequent detection of photoacoustic transients (IVPA imaging) and probing the arterial walls in ultrasound pulse-echo mode (IVUS imaging). The first concepts of an integrated IVUS/IVPA imaging catheter, consisting of a single element ultrasound transducer combined with a custom single optical fiber-based light delivery system,[20] were successfully evaluated in tissue-mimicking phantoms.[21,22] Furthermore, a miniaturized intravascular catheter has been fabricated and tested in *ex vivo* intravascular imaging of human coronary atherosclerosis.[13] In addition, several other designs of the intravascular catheters based on microoptics and utilizing different types of transducers have been proposed.[23,24] However, the feasibility of *in vivo* combined IVUS/IVPA imaging has not yet been investigated.

Translation of IVPA imaging into clinical environment faces several challenges. First, imaging contrast and depth could be limited due to the attenuation of light caused by significant light scattering and absorption of luminal blood.[25] Although removing of the luminal blood during imaging is possible, it is not desirable because it could cause ischemia due to removal of oxygen-carrying hemoglobin, and fluid overload and pulmonary edema due to injecting an additional volume.[26] Previously, it was demonstrated in phantom studies that a prototype of the integrated IVUS/IVPA imaging catheter can be used for IVPA imaging in the presence of blood-mimicking solutions in a lumen while maintaining an imaging depth of several millimeters.[22] Also, the feasibility of 700-nm photoacoustic imaging of an artery with lipid-rich plaques in the presence of luminal blood in the forward imaging mode has been demonstrated *ex vivo*.[27] Later, the *ex vivo* photoacoustic imaging of lipid-rich plaques in a human artery has been performed at 970 and 1200 nm using similar imaging setup.[4] And finally, the

Address all correspondence to: Stanislav Emelianov, University of Texas at Austin, Department of Biomedical Engineering, 1 University Station C0800, Austin, Texas 78712. Tel: 512-471-1733; Fax: 512-471-0616; E-mail: emelian@mail.utexas.edu.

prototype of the integrated IVUS/IVPA imaging catheter has been used for combined IVUS/IVPA imaging of lipids in the presence of whole blood *ex vivo* at 1720 nm.[28] These studies indicated that the presence of luminal blood during IVPA imaging can affect the choice of optical wavelength that provides the best photoacoustic contrast with minimum attenuation of light as it propagates through lumen. Second, *in vivo* combined IVUS/IVPA imaging has to be real time (or at least near real time) to avoid or reduce motion artifacts due to heartbeat and breathing and to allow unambiguous image interpretation. In addition, fast imaging will allow visualization of sufficiently long segments of vessels within a clinically acceptable time period. Real time ultrasound-guided IVPA imaging requires the laser source operating with an appropriate pulse repetition frequency of several kHz. Third, the integrated IVUS/IVPA imaging catheter should be less than 2 mm in diameter to fit a standard, clinically available introducer and to reach deeply into the body. An example of such a small catheter with the diameter of 1.25 mm has been demonstrated in *ex vivo* experiments.[13] Furthermore, the intravascular catheter should be capable of reliable and uniform rotation. All of the above requirements and challenges should be addressed before the combined IVUS/IVPA imaging can be successfully demonstrated for *in vivo* imaging of human coronary arteries.

Here we demonstrate the feasibility of *in vivo* IVUS/IVPA imaging. Furthermore, we demonstrate that IVUS/IVPA imaging is possible in the presence of luminal blood. A coronary stent deployed into a healthy rabbit's thoracic aorta was chosen as an imaging target. Stent imaging is necessary during both its deployment, to ensure appropriate contact between the stent and lumen walls, and its postsurgery follow-up, to investigate the presence of in-stent restenosis,[29] stent drift malapposition,[30] late stent thrombosis,[31] etc. However, IVUS imaging of stents does not exhibit a high contrast between metallic struts of the stent and soft tissues.[32] In this study, the stent was imaged *in vivo* using a modified integrated IVUS/IVPA imaging catheter[21] without the removal of luminal blood. Overall, results of this first *in vivo* IVPA imaging experiment show that integrated IVUS/IVPA imaging catheters suitable for *in vivo* imaging can be designed and fabricated. Future directions to improve the design and performance of the IVUS/IVPA imaging catheter are also discussed.

2 Materials and Methods

2.1 Animal Model

A 2-year-old healthy New Zealand white rabbit was used for *in vivo* imaging. The rabbit was anesthetized using acepromazine and xylazine and placed on a Hallowell ventilator with induction of 2% isoflurane and oxygen. Then, an eight French introducer was inserted into the thoracic aorta. A balloon-expandable off-the-shelf coronary stent (Liberté™, Boston Scientific, Inc.) was deployed into the thoracic aorta to an inner diameter of around 4.5 mm as confirmed by IVUS imaging (Galaxy-2, Boston Scientific, Inc.). The size of the imaged artery is similar to the typical sizes of healthy human coronary arteries, reported as 4.5 mm and 3.9 mm for left and right coronary arteries, respectively.[33] Finally, an integrated IVUS/IVPA imaging catheter was placed into the thoracic aorta through the same eight French introducer. No removal of the luminal blood was applied during the combined IVUS/IVPA imaging.
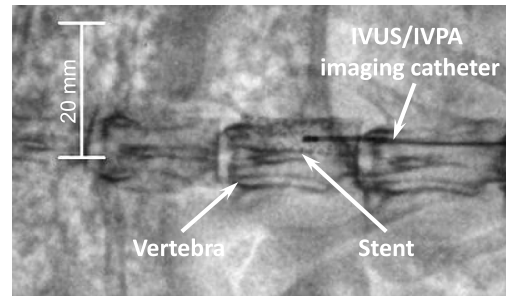

Fig. 1 X-ray image of a rabbit with deployed stent and integrated IVUS/IVPA imaging catheter advanced inside the thoracic aorta. The tip of the catheter is located approximately in the middle of the stent.

Before IVUS/IVPA imaging, the distal end of the integrated catheter was introduced inside the stented area guided by X-ray fluoroscopy (Fig. 1). In the experiments, the rabbit was placed on its back and the coronary stent shown in Fig. 1 situated above the spinal cord. Due to poor contrast of x-ray imaging, the metallic stent cannot be distinguished from the bone reliably and almost coalesces with the vertebra. Also, only metallic components of the integrated IVUS/IVPA imaging catheter are visualized by x-ray imaging thus making a noticeable diameter of integrated IVUS/IVPA imaging catheter smaller than it is.

2.2 Integrated Intravascular Ultrasound and Photoacoustic Imaging Catheter

The diagram and photograph of the integrated IVUS/IVPA imaging catheter are shown in Fig. 2. The integrated catheter consists of a commercially available IVUS imaging catheter (Atlantis™SR plus, Boston Scientific, Inc.)[34] and a customized light delivery system. The central frequency and the fractional bandwidth of the IVUS catheter are 40 MHz and 37%, respectively. The light delivery system is based on a single 1.7-m-long optical fiber (FIP600660710, Polymicro Technologies, Inc.) with core and outer diameters of 0.6 and 0.71 mm, respectively. The light delivery system is constructed based on the effect of total internal reflection as described in detail previously.[21] The distal tip of the fiber was polished at an angle of 30 deg and covered by a gas-trapping cup consisting of a quartz pipe sealed with epoxy. At the distal end of the integrated IVUS/IVPA imaging catheter, the IVUS catheter and the light delivery system were aligned to ensure the maximum overlapped area between ultrasound and light beams using a custom-made plastic fixture. The length and outer diameter of the fixture were 6 mm and 2.2 mm, respectively. Comparing to the previously reported prototypes,[21,22] the light emitting area was located closer to the ultrasound transducer by making the thickness of the sealing epoxy layer (Devcon, Inc.) less than 0.3 mm [Fig. 2(a)]. Also, the epoxy, used to fix the cup quartz pipe and seal the air near the angle-polished surface of the fiber, was located between the fiber and the pipe to improve the mechanical strength of the construction.

Both the optical fiber and the IVUS imaging catheter outside the plastic fixture were incorporated together using 300-mm-long polyethylene tubing with the inner and outer diameters of 1.4 and 1.9° mm, respectively. The space between the tubing and both the optical fiber and the IVUS catheter was filled with silicon to make the construction sealed and to distribute the rotation moment evenly along the tubing. Finally, epoxy was placed between the fixture and the polyethylene tubing to seal the joint and fix two parts together.
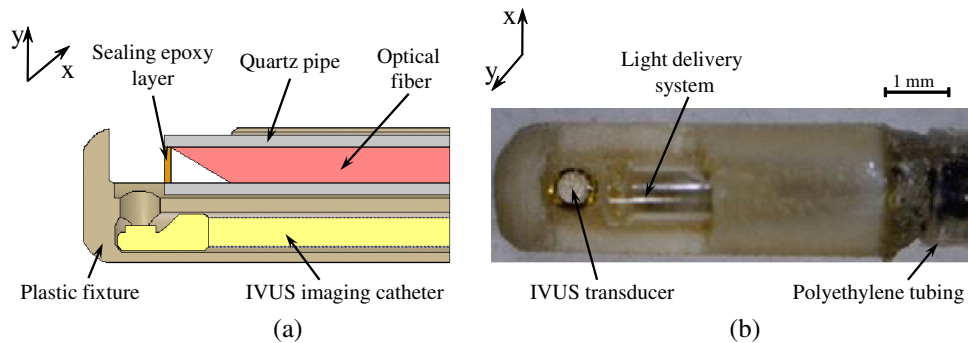
Fig. 2 (a) Schematic diagram and (b) photograph of the integrated IVUS/IVPA imaging catheter used for *in vivo* imaging.

At the proximal end of the integrated IVUS/IVPA imaging catheter, the IVUS catheter was connected to the ultrasound pulser-receiver using a catheter-to-BNC adapter provided by Boston Scientific, Inc. The proximal end of the optical fiber was polished flat and perpendicular to the optical axis of the fiber. The fiber was snugly inserted into a pipe driven by a stepper-motor and coupled with a laser. Smooth and unobstructed rotation of the fully assembled integrated IVUS/IVPA imaging catheter inside a rabbit's thoracic aorta was archived using a custom-made sealed bearing-based rotational adapter.

2.3 Experimental Setup

The block diagram of the experimental setup is shown in Fig. 3(a). A portable Nd:YAG pulsed laser (Polaris II, New Wave, Inc.) with a repetition rate of 20 Hz and pulse duration of 5 ns was operated at 1064 nm wavelength. The laser was coupled with the light delivery system of the catheter.[21] The motor-driven pipe was fixed into two bearings and rotated by a computer-controlled stepper-motor (T-LSR150A, Zaber, Inc.) through the couple of beveled gears. The rotational step size of the catheter was 1.4 deg. The laser energy measured at the distal end of the IVUS/IVPA imaging catheter was 2.5 mJ per pulse. The laser synchronization pulse was used to trigger an

analog-to-digital convertor card (CompuScope 14200, Gage Applied Technologies, Inc.) and an ultrasound pulser-receiver (5073PR, Panametrics-NDT, Inc.). The pulser-receiver operated both in passive (during IVPA receive) and active (during IVUS pulse/receive) mode. To avoid overlapping between photoacoustic transients and ultrasound pulse-echo signals, the ultrasound probing pulses were sent into tissues with a 9 μs delay provided by a delay line (DPR-2515, Directed Energy, Inc.). Both photoacoustic and ultrasound signals were captured by the analog-to-digital convertor card operating at 200 MS/s sampling rate. The obtained dataset was processed off-line.

During *in vivo* combined IVUS/IVPA imaging, the heartbeat can result in motion artifacts. Such artifacts were reduced by electrocardiograph (ECG) gated data acquisition only between QRS complexes. Time diagrams of synchronization pulses at key points of the experimental setup are shown in Fig. 3(b). The laser provided a train of synchronization pulses with a repetition frequency of 20 Hz (time diagram 1). The amplified rabbit's ECG signal (diagram 2) triggered a delay line generating long pulses located between QRS complexes (diagram 3). In the experiments, these long pulses with the duration of 200 ms were generated with the delay of 50 ms in respect to QRS complexes. Both synchronization pulses from the laser (diagram 1)
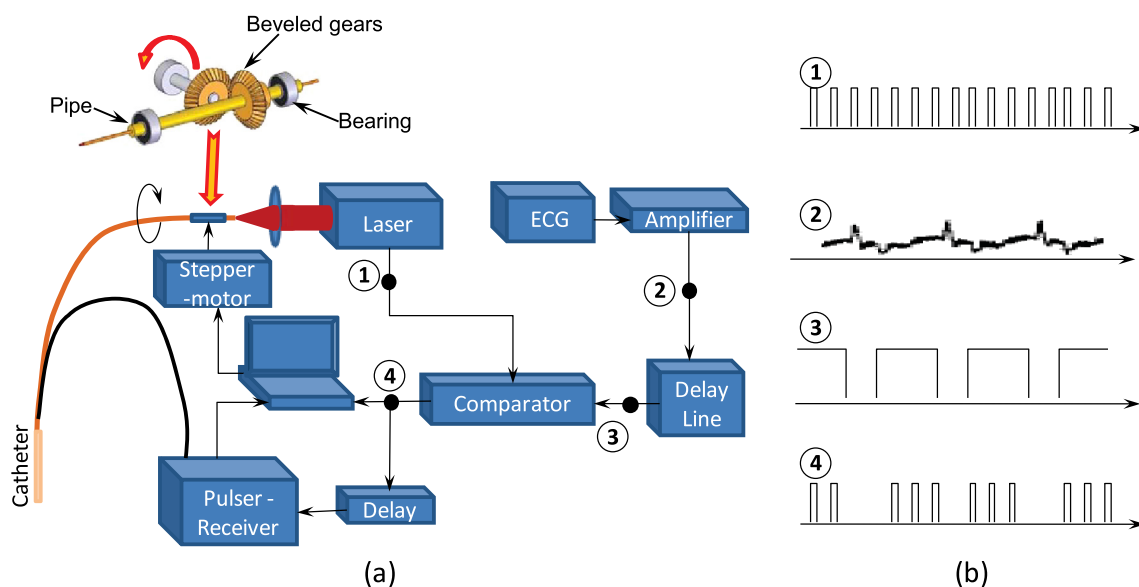

Fig. 3 (a) Schematic diagram of the experimental setup for combined IVUS/IVPA imaging *in vivo*. ECG signals were used to avoid registration of experimental data during QRS complexes. (b) Time diagrams of the synchronization pulses for IVUS/IVPA imaging: (1) triggering pulses from the laser with PRF of 20 Hz, (2) amplified ECG signal, (3) ECG gating, (4) triggering pulses to launch data acquisition and pulser-receiver.
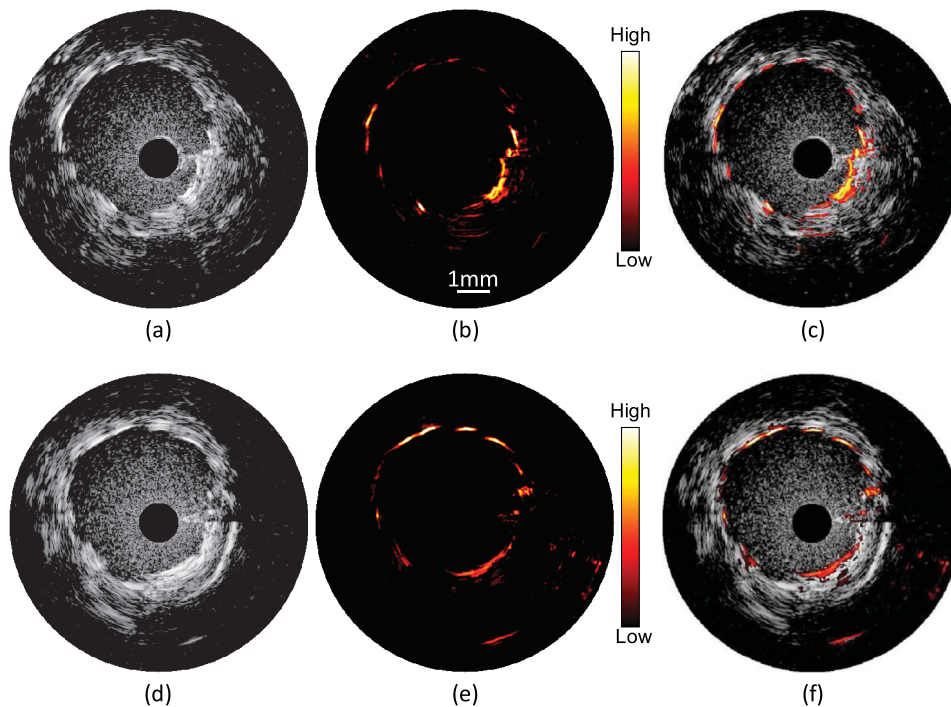
Fig. 4 *In vivo* IVUS (a and d), IVPA (b and e) and combined IVUS/IVPA (c and f) images of the rabbit thoracic artery with a deployed stent. The images (a)–(c) and (d)–(f) correspond to two different cross-sections of the rabbit's artery.

and the long pulses from delay line (diagram 3) were directed to a comparator. The comparator excluded triggering of both data acquisition card and pulser-receiver during and immediately after QRS cycles (diagram 4).

2.4 *Image Acquisition and Processing*

Each IVUS and IVPA image consisted of 256 scanning A-lines and each A-line consisted of coregistered photoacoustic and ultrasound radiofrequency (RF) signals followed one after another with a delay of 9 μs. No averaging was applied during the imaging. Given the pulse repetition frequency of the laser, the minimal acquisition time of each dataset is 12.8 s. However, due to the interruption of imaging during QRS complexes, the average data acquisition time was approximately 17 s per cross-sectional dataset.

During the data processing, the coregistered photoacoustic and ultrasound data were extracted from the RF signals. Then, each photoacoustic and each ultrasound RF signal was band-pass filtered in the frequency range of 20 to 50 MHz and converted into analytical signal. Time-gain compensation (TGC) was applied to IVPA images during the scan-converting to compensate light attenuation in the luminal blood. The location of the blood-tissue interface for each A-line was found using maximum absolute values of the ultrasound analytical signals in the area corresponding to luminal blood and arterial tissues. TGC was not applied to compensate light attenuation in the arterial and surrounding tissues. The absolute values of ultrasound and compensated photoacoustic analytical signals were scan-converted into IVUS and IVPA images with a field of view spanning 4.5 mm in radius. Finally, combined IVUS/IVPA images were produced to further demonstrate the location of the stent's struts (IVPA) within the context of the arterial morphology (IVUS).

3 Results

Two sets of *in vivo* IVUS, IVPA and combined IVUS/IVPA images of the coronary stent deployed inside the rabbit's thoracic aorta in the presence of luminal blood are shown in Fig. 4. The images in Fig. 4(a)–4(c) and in Fig. 4(d)–4(f) were obtained at two different locations within the rabbit's stented artery. The anatomy of the aorta and connective tissues are clearly visible in both IVUS images shown in Fig. 4(a) and 4(d) using 30 dB display dynamic range. Speckles inside the lumen indicate the presence of blood while the black circle in the center indicates the location of the integrated IVUS/IVPA imaging catheter. However, the IVUS contrast between the metallic struts and soft tissues is poor. IVPA images of the same cross-sections of the artery are shown in Fig. 4(b) and 4(e) using a linear display dynamic range. The struts of the stent are clearly depicted while both blood and arterial tissues do not provide noticeable photoacoustic transients due to the high optical absorption coefficient of metal[35] compared to that of soft tissues[36] and blood[25] at 1064 nm wavelength. Such high optical contrast indicates that the laser energy can be potentially decreased to decrease laser fluence without sacrificing the quality of IVPA images. The combined IVUS/IVPA images shown in Fig. 4(c) and 4(f) indicate that highly absorbing areas (struts of the stent) are located at the inner surface of the lumen. The obtained results are in agreement with our previously reported *exvivo* studies.[37]

The brightness of struts in Fig. 4(b) and 4(e) is not uniform. Struts located 9 through 10 o'clock in Fig. 4(b) appear brighter than those located 11 through 12 o'clock in the same image while light propagates similar distance in luminal blood. Meanwhile, brightness of the struts at the same location 10 through 2 o'clock in Fig. 4(e) differs from that in Fig. 4(b) while it was the same stent imaged. The reason is that the cross-section of artery imaged by the integrated IVUS/IVPA imaging catheter was not absolutely perpendicular to the longitudinal axis of

the artery such that both single struts and strut's junctions could be shown in the same image and in the same location of different images. Obviously, a junction of two struts is expected to provide greater photoacoustic signal magnitude than a single strut. In addition, the orientation of the integrated catheter with respect to the vessel wall results in angle variations between the ultrasound beam and different struts during the rotation of the catheter. It was demonstrated that the increased angle may result in a decrease in the IVPA signal magnitude.[38]

4   Discussion

The feasibility of *in vivo* combined IVUS/IVPA imaging using an integrated IVUS/IVPA imaging catheter has been demonstrated. Compared to other interventional optical-based imaging methods, such as optical coherent tomography, *in vivo* IVPA imaging can be realized without temporal removing of the luminal blood. A coronary stent deployed into the thoracic aorta of a rabbit has been successfully visualized using *in vivo* combined IVUS/IVPA imaging. Axial and lateral resolutions of *in vivo* IVPA imaging were found to be similar to that of IVUS imaging. Rabbit's respiration and motion of the artery due to blood pressure changes between the QRS cardio complexes did not result in significant motion artifacts in the images. Therefore, *in vivo* IVPA imaging can supplement conventional clinical IVUS imaging by enabling characterization of arterial tissues and metal implants based on unique optical absorption properties.

Clearly, current design of the integrated IVUS/IVPA imaging catheter fits the thoracic aorta of a healthy rabbit with a diameter of 4.5 mm (Fig. 4) and potentially can also fit both left and right human coronary arteries with typical diameters of 4.5 mm and 3.9 mm, respectively.[33] However, current implementation of the catheter design results is an oversized device that needs to be miniaturized. The concept of possible future design of the integrated IVUS/IVPA imaging catheters has been introduced and discussed elsewhere.[22] Compared to current design where the light delivery system is placed above the IVUS imaging catheter (Fig. 2), a single element ultrasound transducer should be located next to the tip of the optical fiber on the same level. Further improvement should also include a modification of gas-trapping at the distal end of the optical fiber. Instead of the sealed quartz pipe, gas can be trapped by a fixture that covers the fiber tip from all sides excluding the area where light is emitted. That area should be covered by a semi-cylindrical glass or quartz unit sealed to the fixture. This modification will simplify the construction of the catheter, decrease its thickness, and improve the catheter's flexibility. The low laser energy utilized in the experiments allows using the optical fiber with 300-μm-core diameter instead of current 600-μm-core diameter fiber resulting in further decrease of the diameter of the catheter and making the catheter more flexible. Both coaxial wires connecting the ultrasound transducer to the pulser/receiver and the optical fiber should be embedded into a drive cable. Finally, the fully assembled catheter should be placed into plastic tubing with a port for guide wire. After all these improvements, the diameter of the fully assembled integrated IVUS/IVPA imaging catheter is estimated to be 1.0 to 1.2 mm and become comparable with that of regular IVUS imaging catheters. Although a smaller size IVUS/IVPA catheter has been demonstrated,[13] the miniaturization of the integrated IVUS/IVPA imaging catheter remains an active area of investigation.

In these pilot combined IVUS/IVPA imaging experiments, a coronary stent was used as an imaging target to demonstrate the

feasibility of *in vivo* imaging. However, combined IVUS/IVPA imaging has several other unique applications such as characterization of plaque composition and molecular imaging.[16] For example, the IVUS-guided spectroscopic IVPA imaging has been used to image lipids *ex vivo* such that the whole volume of lipid pools can be shown.[13,19] Using nanoparticle-based contrast agents with specific light absorption properties allowed imaging of macrophages in atherosclerotic plaques in an excised artery.[15,39]

In the current studies, 1064 nm wavelength was chosen because of the availability of compact laser source capable of providing sufficient energy per pulse. The IVPA imaging of metallic struts does not require any specific choice of wavelength in the near-IR spectral region due to the wide absorption band of metals and the high optical contrast between metal and soft tissues even in the presence of luminal blood. However, other important clinical applications of the combined IVUS/IVPA imaging are detection of the lipid-rich atherosclerotic plaques and visualization of molecular/cellular events within atherosclerotic plaques using nanoparticle- or dye-based contrast agents with unique molecular/cellular targeting and light absorption properties.[15,40,41] The combined IVUS/IVPA imaging of lipids has been successfully demonstrated at the wavelengths 1210 nm[13,19] and at 1720 nm[28] where the optical absorption coefficient of lipid exceeds that of water.[42] Combined IVUS/IVPA imaging of *ex vivo* lipid-rich plaques in the presence of whole blood in the forward imaging mode[4] and using integrated IVUS/IVPA imaging catheter[28] has been achieved. While using the absorption band around 1210 nm required a sophisticated, time-consuming spectroscopic IVPA imaging even with saline in a lumen,[19] absorption band around 1720 nm is significantly higher and offers a prospect of a single wavelength imaging.[28] Indeed, while the effective attenuation coefficient in blood at 1720 nm is approximately 2.2 times greater than that at 1210 nm, the light absorption coefficient of lipid at 1720 nm is around five time greater that at 1210 nm thus increasing the photoacoustic contrast at 1720 nm and eliminating a need to suppress nonlipid background IVPA signals.[25,42] Overall, the reported prototype of the integrated IVUS/IVPA imaging catheter is based on an optical fiber capable of delivering light in the wide spectral range from 380 to 2400 nm which makes it suitable for all these intravascular applications.

Frame rate of *in vivo* IVPA imaging in our experiments was limited by the pulse repetition frequency of a laser. To achieve *in vivo* real-time (i.e., 30 frames per second) IVPA imaging based on current system configuration (256 scanning A-lines and no averaging), a laser system operated at approximately 7.5 kHz pulse repetition frequency is required. Q-switched diode-pumped solid state (DPSS) Nd:YAG lasers operating at about 10 kHz pulse repetition frequency and providing several mJ of energy per pulse at 1064 nm are currently available from several sources. Such lasers can be utilized if the nanoparticles with maximum light absorption at 1064 nm are used[43] or metallic implants such as stents are imaged. Interestingly, an OPO optimized for operation at fixed wavelength of 1720 nm is usually pumped by the fundamental harmonic of DPSS Nd:YAG laser at the wavelength of 1064 nm. Therefore, one DPSS-based optical system can be potentially used for combined IVUS/IVPA imaging of nanoparticles-based contrast agents and stents at 1064 nm and of lipid at 1720 nm. The DPSS-based laser system will also allow removing the ECG gating during the data acquisition thus allowing the motions

of arteries to be shown in real time as it is typically seen in clinical IVUS imaging.

5   Conclusion

The feasibility of *in vivo* combined IVUS/IVPA imaging using integrated IVUS/IVPA imaging catheter has been successfully demonstrated. In the reported pilot studies, a coronary stent deployed into a rabbit's thoracic aorta was imaged without removing the luminal blood. Both resolution and imaging depth of the *in vivo* IVPA imaging is comparable with that of IVUS imaging. Overall, the results indicate that the concept of integrated IVUS/IVPA imaging catheter is suitable for *in vivo* imaging of metallic implants and vascular tissues.

References

1. S. E. Nissen and P. Yock, "Intravascular ultrasound: novel pathophysiological insights and current clinical applications," *Circulation* **103**(4), 604–616 (2001).
2. R. K. AI Dhahir, P. E. Dyer, and Z. Zhu, "Photoacoustic studies and selective ablation of vascular tissue using a pulsed dye laser," *Appl. Phys. B* **51**(1), 81–85 (1990).
3. T. Allen et al., "Spectroscopic photoacoustic imaging of lipid-rich plaques in the human aorta in the 740 to 1400 nm wavelength range," *J. Biomed. Opt.* **17**(6), 061209 (2012).
4. T. J. Allen et al., "Photoacoustic imaging of lipid rich plaques in human aorta," *Proc. SPIE* **7564**, 75640C (2010).
5. P. C. Beard and T. N. Mills, "Characterization of post mortem arterial tissue using time-resolved photoacoustic spectroscopy at 436, 461 and 532 nm," *Phys. Med. Biol.* **42**(1), 177–198 (1997).
6. M. Xu and L. V. Wang, "Photoacoustic imaging in biomedicine," *Rev. Sci. Instrum.* **77**, 041101 (2006).
7. C. K. N. Patel and A. C. Tam, "Pulsed optoacoustic spectroscopy of condensed matter," *Rev. Mod. Phys.* **53**, 517–550 (1981).
8. A. C. Tam, "Application of photoacoustic sensing techniques," *Rev. Mod. Phys.* **58**(2), 381–431 (1986).
9. S. Sethuraman et al., "Development of a combined intravascular ultrasound and photoacoustic imaging system," *Proc. SPIE* **6086**, 108–117 (2006).
10. S. Sethuraman et al., "Intravascular photoacoustic imaging using an IVUS imaging catheter," *IEEE Trans. Ultrason. Ferroelectr. Freq. Control.* **54**, 978–986 (2007).
11. S. Sethuraman et al., "Ex vivo characterization of atherosclerosis using intravascular photoacoustic imaging," *Opt. Express* **15**(25), 16657–16666 (2007).
12. S. Sethuraman et al., "Spectroscopic intravascular photoacoustic imaging to differentiate atherosclerotic plaques," *Opt. Express* **16**(5), 3362–3367 (2008).
13. K. Jansen et al., "Intravascular photoacoustic imaging of human coronary atherosclerosis," *Opt. Lett.* **36**(5), 597–599 (2011).
14. D. Razansky et al., "Multispectral optoacoustic tomography of matrix metalloproteinase activity in vulnerable human carotid plaques," *Molec. Imag. Biol.* **14**(3), 277–285 (2012).
15. B. Wang et al., "Intravascular photoacoustic imaging of macrophages using molecularly targeted gold nanoparticles," *Proc. SPIE* **7564**, 75640A (2010).
16. B. Wang et al., "Intravascular photoacoustic imaging," *IEEE J. Select. Top. Quantum Electron.* **16**(3), 588–599 (2010).
17. B. Wang et al., "Plasmonic intravascular photoacoustic imaging for detection of macrophages in atherosclerotic plaques," *Nano Lett.* **9**(6), 2212–2217 (2009).
18. B. Wang et al., "High sensitivity intravascular photoacoustic imaging of macrophages," *Proc. SPIE* **7177**, 71770M (2009).
19. B. Wang et al., "Detection of lipid in atherosclerotic vessels using ultrasound-guided spectroscopic intravascular photoacoustic imaging," *Opt. Express* **18**(5), 4889–4897 (2010).
20. A. B. Karpiouk, B. Wang, and S. Y. Emelianov, "Development of catheters for combined intravascular ultrasound and photoacoustic imaging," *Proc. SPIE* **7177**, 717724 (2009).
21. A. B. Karpiouk, B. Wang, and S. Y. Emelianov, "Development of a catheter for combined intravascular ultrasound and photoacoustic imaging," *Rev. Sci. Instrum.* **81**(1), 014901 (2010).
22. A. B. Karpiouk, B. Wang, and S. Y. Emelianov, "Integrated catheter for intravascular ultrasound and photoacoustic imaging," *Proc. SPIE* **7564**, 756408 (2010).
23. B. Y. Hsieh et al., "Integrated intravascular ultrasound and photoacoustic imaging scan head," *Opt. Lett.* **35**(17), 2892–2894 (2010).
24. B.-Y. Hsieh et al., "All-optical scanhead for ultrasound and photoacoustic dual-modality imaging," *Opt. Express* **20**(2), 1588–1596 (2012).
25. A. Roggan et al., "Optical properties of circulating human blood in the wavelength range 400-2500 nm," *J. Biomed. Opt.* **4**(1), 36–46 (1999).
26. K. C. Hoang et al., "Use of an oxygen-carrying blood substitute to improve intravascular optical coherence tomography imaging," *J. Biomed. Opt.* **14**(3), 034028 (2009).
27. S. Sethuraman et al., "Intravascular photoacoustic imaging of atherosclerotic plaques—ex vivo study," *Proc. SPIE* **6437**, 1–9 (2007).
28. B. Wang et al., "Intravascular photoacoustic imaging of lipid in atherosclerotic plaques in the presence of luminal blood," *Opt. Lett.* **37**(7), 1244–1246 (2012).
29. H. Eltchaninoff et al., "Balloon angioplasty for the treatment of coronary in-stent restenosis: immediate results and 6-month angiographic recurrent restenosis rate," *J. Am. College. Cardiol.* **32**(4), 980–984 (1998).
30. N. Guo et al., "Incidence, mechanisms, predictors, and clinical impact of acute and late stent malapposition after primary intervention in patients with acute myocardial infarction," *Circulation* **122**(11), 1077–1084 (2010).
31. S. Cook et al., "Incomplete stent apposition and very late stent thrombosis after drug-eluting stent implantation," *Circulation* **115**(18), 2426–2434 (2007).
32. D. J. Clark et al., "Mechanisms and predictors of carotid artery stent restenosis: a serial intravascular ultrasound study," *J. Am. College. Cardiol.* **47**(12), 2390–2396 (2006).
33. J. T. Dodge, Jr. et al., "Lumen diameter of normal human coronary arteries: influence of age, sex, anatomic variation, and left ventricular hypertrophy or dilation," *Circulation* **86**(1), 232–246 (1992).
34. Boston Scientific Inc., "Atlantis RS Pro imaging catheter," http://www.bostonscientific.com (20 August 2012)
35. B. Karlsson and C. G. Ribbing, "Optical constants and spectral selectivity of stainless steel and its oxides," *J. Appl. Phys.* **53**(9), 6340–6346 (1982).
36. S. Prahl, "Tabulated molar extinction coefficient for hemoglobin in water," http://omlc.ogi.edu/spectra/hemoglobin/summary.html (4 March 1998)
37. J. L. Su, B. Wang, and S. Y. Emelianov, "Photoacoustic imaging of coronary artery stents," *Opt. Express* **17**(22), 19894–19901 (2009).
38. J. L. Su et al., "Photoacoustic imaging of clinical metal needles in tissue," *J. Biomed. Opt.* **15**(2), 021309 (2010).
39. K. Douma, R. T. A. Megens, and M. A. M. J. van Zandvoort, "Optical molecular imaging of atherosclerosis using nanoparticles: shedding new light on the darkness," *Wiley Interdisciplinary Rev.: Nanomed. Nanobiotechnol.* **3**(4), 376–388 (2011).
40. Y.-S. Chen et al., "Silica-coated gold nanorods as photoacoustic signal nanoamplifiers," *Nano Lett.* **11**(2), 348–354 (2011).
41. Y.-S. Chen et al., "On stability of molecular therapeutic agents for noninvasive photoacoustic and ultrasound image-guided photothermal therapy," *Proc. SPIE* **7564**, 75641Q (2010).
42. R. R. Anderson et al., "Selective photothermolysis of lipid-rich tissues a free electron laser study," *Lasers Surg. Med.* **38**(10), 913–919 (2006).
43. K. Homan et al., "Prospects of molecular photoacoustic imaging at 1064 nm wavelength," *Opt. Lett.* **35**(15), 2663–2665 (2010).